IEEE Access
Multidisciplinary | Rapid Review | Open Access Journal

Received 15 September 2023, accepted 11 October 2023, date of publication 16 October 2023, date of current version 26 October 2023.

Digital Object Identifier 10.1109/ACCESS.2023.3324691

RESEARCH ARTICLE

Hybrid Model Predictive Control Scheme for Controlling Temperature in Building Under Uncertainties

CHANGHUN JEONG, OLE MAGNUS BRASTEIN, NILS-OLAV SKEIE, AND ROSHAN SHARMA
University of South-Eastern Norway, 3918 Porsgrunn, Norway

Corresponding author: Changhun Jeong (changhun.jeong@usn.no)

ABSTRACT This paper presents a study on temperature control with a heater in a building using Model Predictive Control (MPC) with a focus on addressing two uncertainties: in model and the weather forecast. In previous works, a grey-box model of the building system was developed, and the values of parameters were estimated by the estimation techniques. In this work, based on the model, simulations are conducted comparing four types of MPC controllers: Deterministic MPC, Multistage MPC, Chance-constrained MPC, and hybrid MPC. The hybrid framework integrates the strengths of the multistage and chance-constrained MPCs to achieve conservative performance and increased robustness in constraint satisfaction. The simulations demonstrate that while deterministic MPC may not always guarantee constraint satisfaction, the hybrid framework offers improved robustness by considering uncertainties in model mismatch and uncertain weather forecasts. The 95% confidence region of model uncertainty is used to assess the robustness of simulations. The results show that the hybrid MPC approach is effective in maintaining temperature in the desired range and ensuring constraint satisfaction in controlling the temperature in a building.

INDEX TERMS Chance-constrained MPC, HVAC system, model predictive control, multistage MPC, optimal control, optimization, stochastic MPC, temperature control, uncertain parameter, uncertainty.

I. INTRODUCTION

Commercial and residential buildings account for approximately 30% of the global energy consumption, with a major portion attributed to heating and cooling utilities [1].

While modern construction techniques and insulation materials have significantly reduced energy consumption for heating and cooling purposes, the rate of building renewal remains considerably low. For instance, in France, the annual renewal rate is estimated to be around 1% [2]. Consequently, the importance of effective building energy management systems (BEMS) has increased, as they offer a more feasible solution compared to modifying the building structure using modern construction techniques. Among the various solutions available, model predictive control (MPC) has garnered attention. At each time step, the control input for heating in a building is determined by solving an optimal control problem (OCP). The OCP consists of a predictive model used to forecast future behavior and constraints that must be satisfied during operation. Solving the OCP yields the optimal control input based on the current knowledge. The first control input from the sequence is then applied to the system, and this process is repeated at the next time step [3], [4]. In the context of BEMS, the utilization of MPC provides benefits in terms of both temperature set point tracking and energy consumption minimization [2].

The research focused on employing MPC in BEMS has witnessed substantial activity [5], [6]. The application of MPC for regulating indoor tempeature using both active heating systems and passive solar blinds were investigated [7]. In [8], a comprehensive building model composed of layered models, which they utilized in conjunction with MPC, was developed. Notably, their four-month experimental evaluation demonstrated remarkable energy savings, with thermal energy consumption reduced by 63% and HVAC electric energy consumption reduced by 29%. These findings

The associate editor coordinating the review of this manuscript and approving it for publication was Feiqi Deng.

highlight the significant potential benefits associated with the integration of MPC into BEMS.

The presence of a reliable prediction model is essential for maximizing the benefits derived from MPC. Various modeling approaches have been proposed to capture the thermal behavior of buildings [9]. For instance, a white-box model based on mass and energy balance was developed, incorporating a system of ordinary and partial differential equations specific to a particular building [10]. However, when dealing with complex models, it becomes challenging to identify a large number of required parameters accurately.

An alternative approach for constructing thermal behavior models is the black box approach, which relies solely on measurement data without prior knowledge of the building. Black box models tend to exhibit high prediction accuracy. However, the drawback lies in the difficulty of generalizing such models, as they do not incorporate physical knowledge to define the model structure. Numerous studies have employed the black box approach, utilizing methods such as ARMAX [11], [12] and PLS-R method [13], [14].

Another modeling approach commonly employed is the grey-box modeling method, which combines aspects of both white-box and black-box models [2], [15], [16], [17], [18]. Grey-box models leverage the cognitive understanding of the underlying physics of the system. In the context of building heating, the structure of the model can be represented using thermal networks. Notably, resistor-capacitor circuit models serve as exemplary thermal network models [19]. The grey-box modeling approach offers certain advantages over the white-box approach, such as reduced-order models. However, a notable characteristic of grey-box models is that their parameters are lumped, meaning each parameter represents a combination of multiple physical properties. Consequently, the estimation of these parameters must be based on measured data [20].

Hence, the formulation of grey-box models offers a more streamlined and comprehensive approach to modeling BEMS. Notably, previous research, in [21] and [22], focused on parameter estimation for grey-box models in the context of BEMS. The outcomes of these study yielded a model characterized by low parameter dispersion. Consequently, the developed model exhibited good agreement with measured data, displaying small deviations, approximately 0.5-1.5$^{\circ}C$ for the most case.

To address the inherent uncertainties and mismatches in system dynamics, stochastic approaches prove to be valuable. Stochastic MPC leverages probabilistic descriptions of uncertainties to establish chance constraints. These chance constraints require that state and output constraints are satisfied with a predefined level of probability. By incorporating chance constraints, stochastic MPC enables systematic utilization of stochastic uncertainty characterization, allowing for permissible levels of probabilistic violation of constraints. This approach facilitates the systematic exploration of trade-offs between achieving control objectives and ensuring probabilistic constraint satisfaction in the presence of uncertainty [23]. Stochastic MPC has found wide-ranging applications in various domains, including building climate control [7], [24], power generation and distribution [25], chemical processes [26], [27], and vehicle path planning [28], [29]. These applications highlight the versatility and effectiveness of stochastic approaches in addressing uncertainty-related challenges across diverse fields.

However, the epistemic error, which is the mismatch between the model and reality, is not the sole source of uncertainty. Various other uncertainties exist, including exogenous disturbances such as external temperature variations from the forecast information. In order to address this uncertainty in the forecast, multistage MPC has emerged as a viable solution [30].

In multistage MPC, the uncertainty is captured through a discrete-time scenario tree that incorporates the future evolution of uncertainty. By considering multiple control trajectories over the scenario tree, multistage MPC accounts for the uncertainty in a robust and proactive manner [32], [33]. The effectiveness and performance of the multistage MPC approach have been demonstrated in various industrial applications, highlighting its applicability and value in practice [30], [31], [33], [34].

Hence, this paper proposes a hybrid MPC framework which incorporates both stochastic MPC and multistage MPC approaches to address two distinct sources of uncertainty: the model uncertainty and the uncertain weather forecast information.

This paper aims to implement the proposed hybrid MPC framework, utilizing a grey box model of the building, to effectively control and regulate indoor temperature. By integrating both stochastic MPC and multistage MPC strategies, this framework provides a comprehensive solution to counteract the uncertainties arising from model mismatch and weather forecast discrepancies. The objective is to achieve robust and reliable temperature control inside the building, considering both sources of uncertainty simultaneously.

The paper is organized as follows: Section II provides brief introductions to several key concepts, including MPC, chance-constrained MPC, multistage MPC, and the parameter estimation method for a grey-box model. Section III presents the proposed hybrid MPC approach. In Section IV, the system description, system model, the parameter estimation process, and the formulation of OCPs for the four types of MPC are discussed. Section V covers the simulation setup conditions and presents the corresponding results. Finally, Sections VI and VII offer discussion and conclusion, respectively.

II. PRELIMINARY

In this section, three types of MPC approaches and the parameter estimation technique are briefly described. The description in this section is for general use. More specific use of these approaches for the indoor temperature management

of the building is described later in Section IV-C. The state variable is denoted as x, the control input as u, the exogenous disturbance as w_{E}, and the model uncertainty as w_{M}. The notation $(\cdot)_k^{(j)}$ represents the state, control input, and uncertainty at time sample k and on the j^{th} scenario. The notation $\mathrm{E}[\cdot]$ denotes an expected value. The system matrices are denoted as A and B. The system matrices for model uncertainty and exogenous disturbance are denoted as G_{M} and G_{E}, respectively.

A. MODEL PREDICTIVE CONTROL

MPC, also known as receding-horizon control, is widely employed for advanced control of multi-variable systems with state and control input constraints [3], [4]. Consider a time-invariant linear system in the discrete-time form:

$$x_{k+1} = Ax_k + Bu_k \tag{1}$$

When perfect knowledge of the system is available, MPC involves solving the following OCP at each sampling time k:

$$\begin{aligned}
\text{minimize} \quad & \sum_{k=0}^{N} J_k && \text{(2a)}\\
\text{subject to} \quad & x_{k+1} = Ax_k + Bu_k && \text{(2b)}\\
& Hx_{k+1} \le h && \text{(2c)}\\
& Du_k \le d && \text{(2d)}\\
& x_0 = \hat{x} && \text{(2e)}
\end{aligned}$$

In OCP (2), N represents the length of the prediction horizon. The system model is written in (2b). The state and control inputs are posed in (2c) and (2d). The matrices H and D correspond to the state and input constraint matrices, respectively, with h and d representing the corresponding constraint values. The initial state is given from measurement or estimation as posed in (2e). In the cost function (2a), J_k is commonly chosen as a regularization cost to drive the state and input to zero:

$$J_k = (x_{k+1}^\top Q_x x_{k+1} + u_k^\top R_u u_k) \tag{3}$$

here, $u := \{u_0, u_1, \ldots, u_N\}$ is a sequence of control inputs, and the matrices $Q_x \ge 0$, and $R_u \ge 0$ are weight matrices.

B. CHANCE-CONSTRAINED MPC

Chance-constrained MPC is a well-known stochastic MPC approach that accounts for uncertainties in system dynamics. While the nominal MPC assumes a deterministic evolution of the state x_k, real systems often exhibit uncertainties in model structure and parameters. To incorporate these uncertainties, the system model (1) is modified as follows:

$$x_{k+1} = Ax_k + Bu_k + G_{\mathrm{M}} w_{\mathrm{M},k} \tag{4}$$

here, the disturbances $w_{\mathrm{M},k}$ is assumed to be sequences of independent and identically distributed variables with known probability distribution p_w. Additionally, it is assumed that $\mathrm{E}[w_{\mathrm{M},k} \cdot w_{\mathrm{M},k}^\top] = Q_w$.

Chance-constrained MPC leverages the knowledge of the mean and variance of the predicted state to ensure that state constraint violations remain within acceptable bounds. Given the available system information at time k, chance-constrained MPC aims to minimize the expected value of the cost function (3) while considering a stochastic prediction model for the state, input constraints, and state chance constraints [26], [35]. The Chance-constrained OCP can be formulated as follows [23]:

$$\begin{aligned}
\underset{u}{\text{minimize}} \quad & \mathrm{E}\left[\sum_{k=0}^{N} J_k\right] && \text{(5a)}\\
\text{subject to} \quad & x_{k+1} = Ax_k + Bu_k + G_{\mathrm{M}} w_{\mathrm{M},k} && \text{(5b)}\\
& \Pr[H_c x_{k+1} \le h_c] \ge 1 - \beta_j && \text{(5c)}\\
& Du_k \le d && \text{(5d)}\\
& \mathrm{E}[x_0] = \hat{x}, \quad w_k \sim p_w && \text{(5e)}
\end{aligned}$$

In this OCP formulation, (5c) represents the state chance constraints, where the probability of violating constraint h_c is set by a predefined threshold $\beta_j \in (0, 0.5]$. Notably, the inclusion of the stochastic variable $w_{\mathrm{M},k}$ in the model (5b) does not imply using specific realizations or sequences of disturbance values for prediction. Instead, it involves propagating the mean and variance of the stochastic state through the model equations (5b), which are necessary for evaluating the cost function (5a) and chance constraints (5d).

When the model is linear and the uncertainty follows a Gaussian distribution, the stochastic OCP can be transformed into a similar form to the deterministic MPC. The modified OCP takes the following form [36]:

$$\begin{aligned}
\underset{v}{\text{minimize}} \quad & \sum_{k=0}^{N} J_k^{\mathrm{SMPC}} && \text{(6a)}\\
\text{subject to} \quad & z_{k+1} = Az_k + Bv_k && \text{(6b)}\\
& Hz_{k+1} \le \eta_{k+1} && \text{(6c)}\\
& Dv_k \le d && \text{(6d)}\\
& z_0 = \hat{x} && \text{(6e)}
\end{aligned}$$

where J_k^{SMPC} in Equation (6a) is expressed as:

$$J_k^{\mathrm{SMPC}} = (z_{k+1}^\top Q_x z_{k+1} + v_k^\top R_u v_k) \tag{7}$$

here, z and v represent the deterministic term of the state and perturbations to a static feedback law, respectively. They can be expressed as $x_k = z_k + e_k$ and $u_k = K_{\mathrm{p}} e_k + v_k$, where e_k represents the error at time k and K_{p} is the feedback law constant. In (6c), η_{k+1} is defined as $H_j z_{k+1} \le F_{j,k+1}^{-1}(1-\beta)$, where $F_{j,k+1}^{-1}$ is the inverse cumulative density function (CDF). The difference $h_j - \eta_{k+1}$ represents the constraint back-off magnitude, indicating how much the predicted value $H_j z_{k+1}$ needs to back off from the original bound h_c to satisfy the chance constraint (5c). When $w_{\mathrm{M},k}$ is Gaussian, computing η_{k+1} is straightforward. Given $x_k \sim \mathcal{N}(z_k, \Sigma_k)$, the state covariance can be propagated over the prediction horizon as $\Sigma_{k+1} = A\Sigma_k A^\top + GQ_w G^\top$ for $k = 0, 1, \ldots, N-1$.

Consequently, the predicted state x_{k+1} and error e_{k+1} follow Gaussian distributions $x_{k+1} \sim \mathcal{N}(z_{k+1}, \Sigma_{k+1})$ and $e_{k+1} \sim \mathcal{N}(0, \Sigma_{k+1})$, respectively. Since $He - h$ is a linear transformation of the Gaussian random variable e, the CDFs $F_{j,k+1}$ and their inverses can be computed from the probability distribution function of $He_{k+1} - h$. For further details, refer to [36].

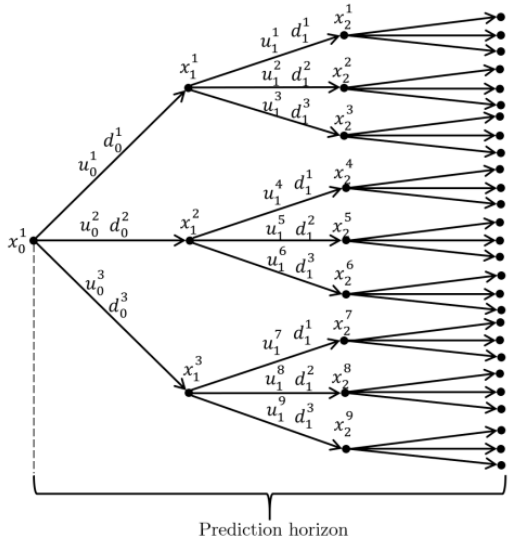

FIGURE 1. The structure of the scenario tree [33].

C. MULTISTAGE MPC

Multistage MPC employs a form of scenario tree, as shown in Figure 1, to describe the uncertainty. The control inputs are optimized to counteract uncertainties in the tree. When implementing multistage MPC, all control inputs branching at the same node must be equal. These equal control inputs are imposed by non-anticipativity constraints [33].

The time-invariant linear system model with exogenous disturbance can be written as:

$$x_{k+1} = Ax_k + Bu_k + G_{\mathrm{E}} w_{\mathrm{E},k} \tag{8}$$

The OCP of multistage MPC can be formulated as follows:

$$\underset{u}{\text{minimize}} \sum_{j=1}^{S} \omega_j \sum_{k=0}^{N} J_k^j \tag{9a}$$

$$\text{subject to} \quad x_{k+1}^j = Ax_k^{p(j)} + Bu_k^j + G_{\mathrm{E}} w_{\mathrm{E},k}^{r(j)} \tag{9b}$$

$$Hx_{k+1}^j \leq h \tag{9c}$$

$$Du_k^j \leq d \tag{9d}$$

$$u_k^j = u_k^l, \quad \text{if} \quad x_k^{p(j)} = x_k^{p(l)} \tag{9e}$$

$$x_0^j = \hat{x} \tag{9f}$$

In this formulation, ω_j represents the weight or importance of the j^{th} scenario. The system model is given in (9b). Here, $x_k^{p(j)}$ means the parent node state where the scenario is branching out, and $w_{\mathrm{E},k}^{r(j)}$ is the realization of the uncertainty scenarios on current time. The state and the control bounds are posed in (9c) and (9d), respectively. The non-anticipativity constraint is given in (9e). Here, j and l denote different scenarios. The initial condition is set in (9f).

In multistage MPC, the size of the optimization problem can grow exponentially with the length of the prediction horizon, the number of uncertainties, and the number of branches from each parent node. To address this challenge, a technique called robust horizon is often employed, which limits the branching of scenarios up to a certain stage while assuming the later uncertainties to be constant. This approach provides a compromise between handling uncertainties and computational efficiency [33].

D. GREY-BOX MODEL AND PARAMETER ESTIMATION

The process of parameter identification through numerical optimization has been extensively studied in the literatures [2], [18], [37]. Optimization algorithms are commonly employed to minimize an objective function, which in the context of parameter estimation, typically represents the discrepancy between model predictions and reference data. The objective function is based on the simulation error computed over the entire calibration period, as opposed to the traditional one-step-ahead prediction errors commonly used in statistical approaches [12], [38]. This approach can be seen as a least squares curve fitting procedure. Consequently, the objective function is defined as the mean square error (MSE) between simulated and measured states over the entire dataset. The chosen error function is a standard quadratic norm [39], expressed as:

$$J = \sum_{i=1}^{N} \sum_{k=1}^{n_x} e_k^2 = \sum_{i=1}^{N} \sum_{k=1}^{n_x} (x_k^i - x_k^{i,ref})^2 \tag{10}$$

where n_x denotes the number of states and N is the number of samples in the dataset. The sum of squared errors for each temperature state is accumulated, with equal weighting assigned to all states. Alternatively, it is possible to assign weights based on the uncertainties associated with the measurements, such as the covariance of the measurements, as commonly practiced in statistical approaches to parameter estimation [38].

III. HYBRID MPC

The hybrid MPC approach is developed to address two sources of uncertainties separately: model mismatch and exogenous disturbance. The model mismatch is quantified during the validation step by comparing the model predictions with experimental data, allowing for the characterization of deviations in probabilistic terms. On the other hand, exogenous information is incorporated into the control framework through a scenario tree, which can be constructed based on expert opinions or provided prediction information. The model mismatch is handled using a chance-constrained

framework, which relaxes the associated state constraints by specifying an acceptable level of constraint violation. The scenario tree, on the other hand, is integrated into the optimization problem using the multistage MPC framework to counteract the influence of the exogenous disturbance. By combining these two frameworks, the following OCP for the hybrid MPC is formulated:

$$\underset{u}{\text{minimize}} \quad \sum_{j=1}^{S} \omega_j \mathrm{E}\left[\sum_{k=0}^{N} J_k\right] \tag{11a}$$

$$\text{subject to} \quad x_{k+1}^{j} = A x_k^{p(j)} + B u_k^{j} + G w_k^{r(j)} \tag{11b}$$

$$\Pr[H_c x_{k+1}^{j} \le h_c] \ge 1 - \beta_j \tag{11c}$$

$$D u_k^{j} \le d \tag{11d}$$

$$u_k^{j} = u_k^{l} \quad \text{if} \quad x_k^{p(j)} = x_k^{p(l)} \tag{11e}$$

$$\mathrm{E}[x_0^{j}] = \hat{x}, \quad wk \sim p_w \tag{11f}$$

In this formulation, the system dynamics are captured by the state equation (11b), where $Gw_k^{r(j)}$ describes the uncertainty at time step k on j^{th} scenario as $Gw_k^{r(j)} = G_{\mathrm{M}} w_{\mathrm{M},k}^{r(j)} + G_{\mathrm{E}} w_{\mathrm{E},k}^{r(j)}$. The chance constraint (11c) ensures that the state satisfies the hard constraint $H_c xk + 1^j \le h_c$ with a probability of at least $1 - \beta_j$. The control bounds are given by (11d). The non-anticipativity constraint (11e) ensures that the control inputs are equal if the corresponding states are equal. The initial state is specified by (11f), where $\hat{x}$ represents the measured or estimated initial state and $w_{\mathrm{M},k}$ is a random variable following the distribution p_w. The objective is to minimize the expected cost over the entire scenario $\sum_{j=1}^{S} \omega_j \mathrm{E}\left[\sum_{i=0}^{N} J_k\right]$ by selecting appropriate control inputs u_k^{j}.

Overall, the hybrid MPC approach counteracts both model mismatch and exogenous disturbance effectively, providing an ability to handle uncertainties in real-world systems.

If the model uncertainty is expressed in the form of a Gaussian distribution and the model is linear, the OCP for hybrid MPC can be written as:

$$\underset{u}{\text{minimize}} \quad \sum_{j=1}^{S} \omega_j \sum_{k=0}^{N} J_k^{j,\mathrm{SMPC}} \tag{12a}$$

$$\text{subject to} \quad z_{k+1}^{j} = A z_k^{j} + B v_k^{j} + G w_k^{r(j)} \tag{12b}$$

$$H z_{k+1}^{j} \le \eta_{k+1} \tag{12c}$$

$$D v_k^{j} \le d \tag{12d}$$

$$v_k^{j} = v_k^{l} \quad \text{if} \quad z_k^{p(j)} = z_k^{p(l)} \tag{12e}$$

$$z_0^{j} = \hat{x} \tag{12f}$$

IV. SYSTEM DESCRIPTION

The building in this study is an experimental setup constructed in 2014 at the Porsgrunn campus of the University of South-eastern Norway [40]. The exterior and floor plan of the test building is depicted in Figure 2. The building is designed with concrete support structures, ensuring that it remains detached from the ground. The internal volume of the building is approximately 9.4 m^3, and it is sealed without both natural and mechanical ventilation systems. To limit solar irradiation, three small windows measuring 60×90 cm^2 are positioned in the south, east, and west directions, while a 90×120 cm^2 door is located in the north direction. Additionally, the presence of three surrounding buildings further restricts the amount of solar radiation entering through the windows.

The building envelope is constructed using a combination of different materials, including wooden cladding, glass wool, air-fill, polyethylene vapor barriers, wood, cement chipboard, particleboard, and cardboard. Each type of wall exhibits a unique construction, resulting from the combination of these materials. Similarly, the roof and floor of the building have distinct compositions.

The experimental building features an electrical heater with a power rating of 375 W, comprising a thermostat controller, a measurement system, and a logging computer consuming approximately 100 W. The measurement system incorporates various sensors to monitor parameters such as indoor and outdoor temperatures and humidity, air pressures, rainfall, wind speed, wind direction, and total power usage.

Overall, the experimental building serves as a controlled environment for studying and analyzing the thermal dynamics and energy performance of buildings under different operating conditions.

A. SYSTEM MODEL

The chosen system model in this study offers a simplified representation of the experimental building, serving as the source of calibration data. Illustrated in Figure 3, the model is founded on the R3C2 model employed in a previous study [2]. Notably, the ventilation resistance component is omitted from this model due to the absence of a ventilation system in the test building.

The model encompasses two state variables: T_{b}, representing the interior temperature of the building, and T_{w}, signifying the temperature of the wall's inner surface. The control input, denoted as $\dot{Q}$, accounts for the heat flow source (e.g., an electric heater). Two sources of uncertainty are inherent in this model. Firstly, model uncertainty, characterized by w_{b} and w_{w}, arises from the stochastic mismatch between model predictions and actual observations. The model mismatch can occur due to various factors such as wind, sunlight and so on. Secondly, external temperature variations and weather forecast scenarios are denoted as T_∞.

To capture the building's thermal properties, capacitors C_{b} and C_{w} are integrated into the model, representing thermal energy storage capacities within the interior and the building envelope (comprising walls, floor, and ceiling). Furthermore, the model incorporates three resistance components: R_{b}, symbolizing the thermal resistance between the building interior and the wall; R_{w}, representing the resistance to heat flow through the wall, connecting state T_{w} with the outside temperature; and R_{g}, characterizing heat flow resistance through

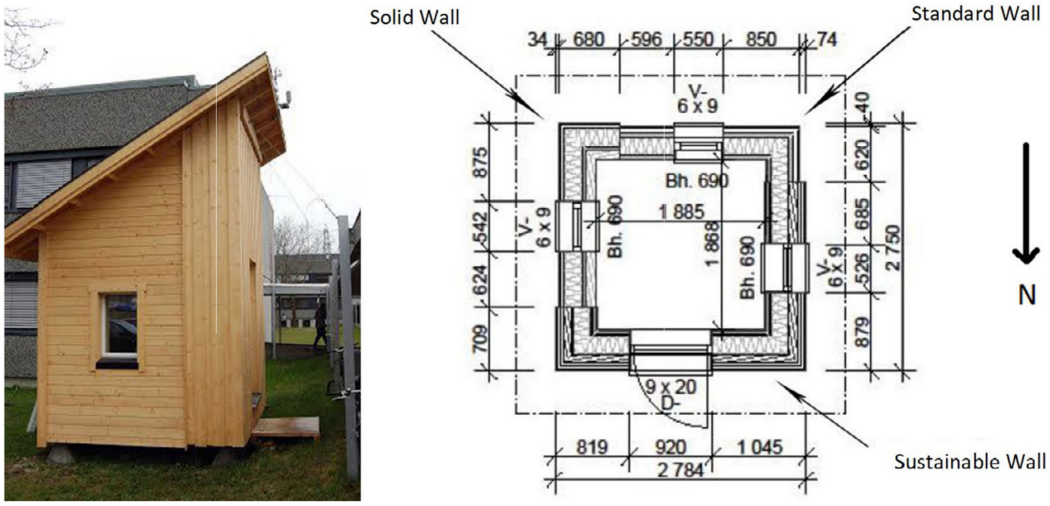

FIGURE 2. The picture of the experimental facility in USN [40].

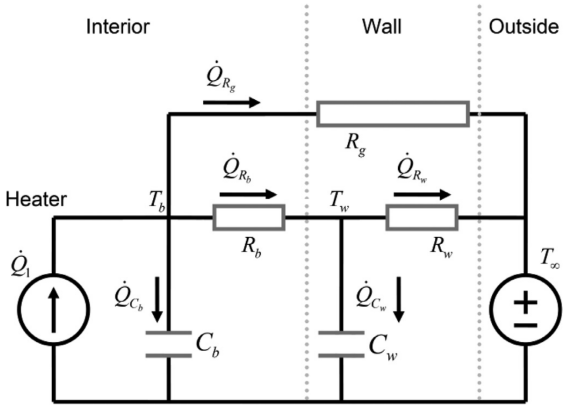

FIGURE 3. RC circuit model of the building [22].

unaccounted components of the building envelope, such as windows and doors.

To derive equations from this thermal network model, Kirchhoff's node potential law is employed. In this approach, each state (T_b and T_w) is assigned to a circuit node, ensuring a balanced flow into and out of each node. Consequently, the stochastic model can be expressed as a set of following ordinary differential equations (ODEs): [21], [22], [39].

$$\frac{dT_b}{dt} = -\left(\frac{1}{C_\mathrm{b}R_\mathrm{b}} + \frac{1}{C_\mathrm{b}R_\mathrm{g}}\right)T_b + \left(\frac{1}{C_\mathrm{b}R_\mathrm{b}}\right)T_w + \left(\frac{1}{C_\mathrm{b}}\right)\dot{Q} + \left(\frac{1}{C_\mathrm{b}R_\mathrm{g}}\right)T_\infty + w_\mathrm{b} \tag{13}$$

$$\frac{dT_w}{dt} = \left(\frac{1}{C_\mathrm{w}R_\mathrm{b}}\right)T_b - \left(\frac{1}{C_\mathrm{w}R_\mathrm{w}}\right)T_w + \left(\frac{1}{C_\mathrm{w}R_\mathrm{w}}\right)T_\infty + w_\mathrm{w} \tag{14}$$

In the context of this analysis, an assumption emerges regarding the determinism of the model under specific conditions. Specifically, assuming constant and unchanging model uncertainties, denoted as w_b and w_w, and further presuming perfect knowledge and precision in the external temperature variable T_∞ as applied in equations (13) and (14), the model takes on a deterministic form.

The deterministic model operates without the presence of randomness or variability associated with the model uncertainties and external temperature fluctuations. This simplification enables a more predictable and precise analysis, which can be advantageous when these assumptions align with the specific research or practical context in question. However, it is crucial to acknowledge that the deterministic model relies on these stringent assumptions and may not fully capture the real-world complexities inherent in many practical scenarios.

B. PARAMETER ESTIMATION

The parameter estimation in this building is previously done in [21] and [22]. The process of parameter estimation involves determining the values of model parameters based on experimental data. In this case study, a nominal parameter vector is employed as an initial approximation for the estimation methods. These nominal values are obtained through trial and error experiments and prior knowledge of the expected parameter range. The physical insight required for these initial approximations is limited to the approximate order of magnitude of the parameters, which can typically be obtained for most practical buildings. The nominal values themselves do not necessarily yield an accurate prediction model for the building, but they serve as normalization constants, allowing parameter estimation to be performed on a unit scale. Moreover, they restrict the search space to a region of interest where reasonable parameter values can be obtained [21], [22].

Table 1 presents a set of nominal parameters obtained through experimental measurements. These values are used as initial guesses for model calibration, and the corresponding minimum and maximum limits define the constrained parameter space [10].

The noise covariance matrix $W = \text{diag}(w_b^2, w_w^2)$ are estimated from the data and assumed to be diagonal. The parameter vector is defined as follows:

$$\theta = [R_g, R_b, R_w, C_b, C_w, w_b, w_w] \tag{15}$$

TABLE 1. Nominal parameter values and min./max. range.

	R_g[K/W]	R_b[K/W]	R_w[K/W]	C_b[J/W]	C_w[J/W]
Nominal value (θ_0)	0.160	0.060	0.100	1200k	1200k
Min value ($\theta_{\min}$)	0.048	0.018	0.03	360k	360k
Max value ($\theta_{\min}$)	0.272	0.102	0.170	2040k	2040k

To prevent over-parameterization, one degree of freedom is removed by fixing the value of R_g to a constant. R_g represents the thermal resistance of windows and doors, which are exposed to both interior and exterior temperatures, and their UA values are specified in [10]. The UA values are calculated as the product of U (the reciprocal of thermal resistance per area) and A (the area). Therefore, knowing R or U for all windows and doors, as well as their areas A, allows for the computation of $R_g = 1/(U_g A_g)$. The specifications for U and A are presented in Table 2, and the value of R_g is set to 0.24 [10], [22].

TABLE 2. Specification of R_g.

	U[W/m^{2}K]	A[m^2]	UA [W/K]	R [K/W]
Door	1.2	1.76	2.1	0.48
Windows	1.3	1.57	2.0	0.50
Total	-	-	4.1	0.24

Using the R3C2 model from Fig. 3, a prior distribution is assigned to the parameter R_g as $\mathcal{N}(0.24, 0.01^2)$, while all other parameters have uniform priors $p(\theta) = 1$. These distributions are employed in optimization calculations with optimization equation (10) [21].

TABLE 3. Values and standard deviations of estimated parameters.

	$\hat{\theta}$	$\sigma/\hat{\theta}$
R_g[K/W]	0.236	6.0%
R_b[K/W]	0.072	5.7%
R_w[K/W]	0.084	5.7%
C_b[J/W]	1444k	4.7%
C_w[J/W]	293k	8.8%
w_b	0.149	3.2%
w_w	0.137	3.7%

The posterior distribution of the parameters is estimated using the Markov Chain Monte Carlo (MCMC) method. Three independent sets of data were collected from the experimental building, including temperature measurements T_b, T_w, and T_∞, as well as one measurement of the input electrical power $\dot{Q}$ supplied to an electric heater. The temperatures T_b and T_w serve as reference data for the model outputs, while T_∞ and $\dot{Q}$ act as the model inputs. Two of the data sets are utilized as training data for parameter estimation and analysis, while the remaining data set is used as a test set solely for evaluating the posterior predictive distribution and assessing the calibrated model's ability to predict future system behaviors. The estimated parameters are presented in Table 3, along with their corresponding standard deviations. The standard deviations are normalized with respect to the maximum a posteriori (MAP) estimates of the parameters, enabling a comparison of different parameters [21], [22].

For a more comprehensive analysis of the parameter estimation in this case study, please refer to [21] and [22].

C. OPTIMAL CONTROL PROBLEM

In this section, the OCPs related to the case study of building temperature control is introduced. The state at time sampling k is denoted as $x_k = [T_{b,k}, T_{w,k}]$. u includes both control input, $\dot{Q}$, and exogenous disturbance, T_∞, as $u_k = [\dot{Q}_k, T_{\infty,k}]$. The model mismatch is described in w_k.

1) DETERMINISTIC MPC WITHOUT CONSIDERING UNCERTAINTIES

In this subsection, the OCP for implementing deterministic MPC is introduced, assuming no model mismatch and perfect forecast in outside temperature. The OCP for deterministic MPC is formulated as follows:

$$\begin{aligned}
\text{minimize} \quad & \sum_{k=0}^{N} J_k && \text{(16a)}\\
\text{subject to} \quad & x_{k+1} = Ax_k + Bu_k && \text{(16b)}\\
& 20^\circ\text{C} \le T_{b,k} + Z_k \le 22^\circ\text{C} && \text{(16c)}\\
& 100\text{W} \le \dot{Q}_k \le 475\text{W} && \text{(16d)}\\
& x_0 = \hat{x} && \text{(16e)}
\end{aligned}$$

In Equation (16a), the cost function is defined, while Equation (16b) represents the system model in deterministic form. The model parameters used are specified in Table 3. The bounds for the building's interior temperature ($T_{b,k}$) and the electricity consumption ($\dot{Q}_k$) are given by Equations (16c) and (16d), respectively. Z_k in (16c) is a slack variable. The minimum electricity consumption in the building is set to 100W due to the use of a computer for data logging. Therefore, when 100W is used, the heater is turned off.

The cost function (16a) is designed in a quadratic form as follows:

$$J_k = T_k W_x T_k^\top + \left(\frac{\dot{Q}_k}{\dot{Q}_{\max}}\right) W_u P_k \left(\frac{\dot{Q}_k}{\dot{Q}_{\max}}\right)^\top + Z_k W_v Z_k^\top \tag{17}$$

In Equation (17), the first term, $T_k W_x T_k^\top$, represents the target temperature term. T_k is the difference between the target temperature and the temperature inside the building at

sampling time k, denoted as $T_{\mathrm{b},k}$. The target temperature is set to 22°C in this work. T_k is mathematically expressed as $T_k = T_{\mathrm{b},k} - 22°\mathrm{C}$.

The second term in Equation (17) represents the power consumption term. $\dot{Q}_k$ denotes the power consumption at time sampling k, and $\dot{Q}_k/\dot{Q}_{\max}$ normalizes the energy usage. P_k is the normalized electricity price over the prediction horizon, expressed as the ratio of the electricity price at sampling time k to the mean price over the prediction horizon.

The last term in Equation (17), $Z_k W_v Z_k^\top$, is a penalty term that allows violations of the constraint (16c) when it cannot be satisfied. Z_k is a slack variable and it is decided by solving optimization. It is encouraged to be zero in most cases.

The parameters W_x, W_u, and W_v are weight parameters for the target temperature term, power consumption term, and penalty for constraint violations, respectively. They are assumed to be positive-definite. By adjusting these parameters, the MPC can control the system differently. For example, if W_x is significantly higher than W_u, the MPC will prioritize controlling the heater to maintain the temperature at the target value with maximum effort. In the opposite case, the MPC will minimize the use of the heater as long as the temperature remains within the constraint (16c). W_v must always be kept significantly higher than the other two parameters for the satisfaction of the constraints.

2) HYBRID MPC: COMBINATION OF MULTISTAGE MPC AND CHANCE-CONSTRAINED MPC

There are two types of uncertainties in the system: exogenous disturbances and model uncertainty. Exogenous disturbances represent uncertainties in weather forecast information. Despite the high accuracy of weather forecasts, deviations between the forecast temperature and the actual temperature are inevitable. Model uncertainty arises from the mismatch between the model and reality, as it is nearly impossible to build a model that precisely represents reality. The uncertainty data can be estimated through experiments, and in this study, the mismatch is shown as w_{b} and w_{w} (refer to Table 3).

The uncertainty in weather forecast information can be mitigated using the multistage MPC framework or scenario-based MPC. The OCP of the multistage MPC framework with the robust horizon set as 1 is formulated as follows:

$$\begin{aligned}
\text{minimize} \quad & \sum_{j=1}^{S} w_j \sum_{k=0}^{N} J_k^{(j)} && \text{(18a)}\\
\text{subject to} \quad & x_{k+1}^{(j)} = A x_k^{(j)} + B u_k^{(j)} && \text{(18b)}\\
& 20°\mathrm{C} \le T_{\mathrm{b},k}^{(j)} + Z_k^{(j)} \le 22°\mathrm{C} && \text{(18c)}\\
& 100\mathrm{W} \le \dot{Q}_k^{(j)} \le 475\mathrm{W} && \text{(18d)}\\
& x_0^{(j)} = \hat{x} && \text{(18e)}\\
& \dot{Q}_0^{(0)} = \dot{Q}_0^{(1)} = \cdots = \dot{Q}_0^{(S)} && \text{(18f)}
\end{aligned}$$

However, in multistage MPC, the uncertainty from model mismatch is not considered. This model uncertainty can be addressed by incorporating the chance-constrained MPC framework. To implement chance constraints, the constraint (16c) can be modified in the OCP (16a) as follows:

$$20°C + e_k \le T_{\mathrm{b},k} + Z_k \le 22°C - e_k \tag{19}$$

To implement the hybrid MPC framework which addresses both uncertainty in model and forecast information, the constraint (18c) can be modified in the OCP (18) as follows:

$$20°C + e_k \le T_{\mathrm{b},k}^{(j)} + Z_k^{(j)} \le 22°C - e_k \tag{20}$$

In the newly proposed constraints (19) and (20), e_k represents the constrained back-off obtained from the inverse cumulative distribution function with the propagated covariance throughout the prediction horizon and pre-defined β. Based on the given w_b and w_w in Table 3 and $\beta \in (0, 0.5]$, the constrained back-off e is defined as shown in Figure 4.

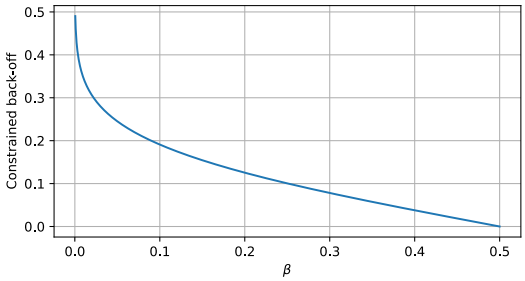

FIGURE 4. The constrained back-off obtained from the inverse CDF for the distribution of $N(0, w_b)$, plotted as a function of the permitted probability of state constraint violation $\beta \in (0, 0.5]$.

V. SIMULATION

A. SIMULATION SETUP

In Norway, the electricity price is determined in advance for the next 24 hours in a deterministic manner and published on the website: **nordpool.no**. Therefore, there is no uncertainty in the electricity price. Figure 5 presents the historical temperature forecast and electricity price.

In simulations, a prediction horizon length is set as 5 hours and a time step is set as 2 minutes. The optimization problem for running MPC is solved using CasADi in Python [41]. In this work, four MPCs are compared, as outlined in Table 4.

TABLE 4. MPCs used in the simulations.

1	Deterministic MPC(D)
2	Multistage MPC(MS)
3	Chance-Constrained MPC(CC)
4	Hybrid MPC(Hybrid)

The simulations are conducted with various sets of weight parameters to demonstrate the effectiveness of each controller. The parameter sets are presented in Table 5 and are selected with trial and error.

To consider the uncertain weather forecast for the implementation of multistage MPC and hybrid MPC, A scenario tree must be built. There are two ways to build a scenario tree. One is to purchase forecast data from third-party companies.

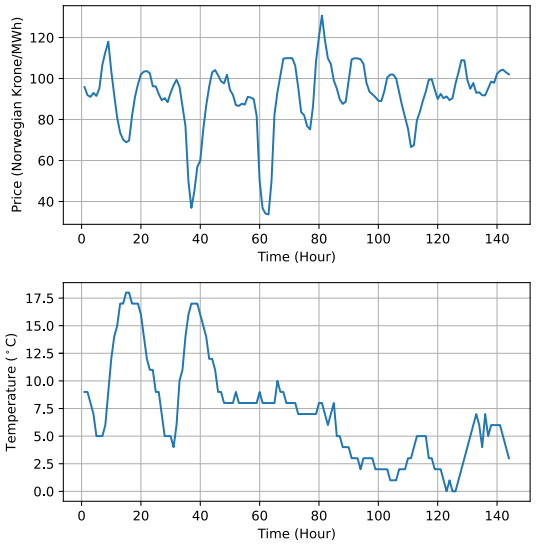

FIGURE 5. Forecast of outside temperature and electricity price.

TABLE 5. Weight parameter sets used in the simulations.

Parameters	A	B	C	D	E
W_x	100	1	0.1	0.05	0.01
W_u	1	1	1	1	1
W_v	10^6	10^6	10^6	10^6	10^6

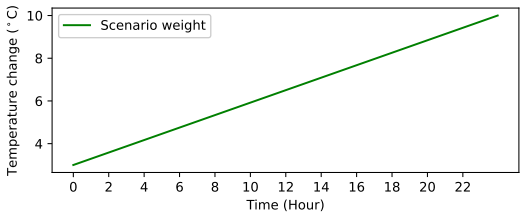

FIGURE 6. The addition and subtraction amounts through the prediction horizon to generate the possible prediction scenarios of the outside temperature.

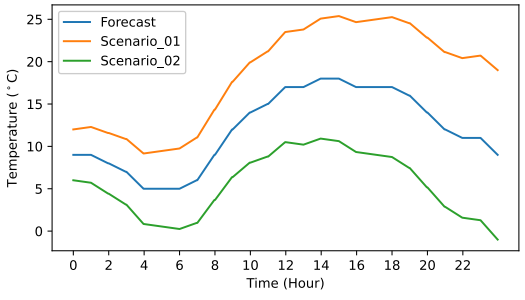

FIGURE 7. The prediction scenario tree of the temperature outside.

The other method is to utilize publicly available weather forecast data and to add or subtract reasonable ranges of temperatures for each time step over the prediction horizon. In this study, the latter method is used in this paper. To generate 2 more possible scenarios from the original forecast data by adding and subtracting the temperature change over the prediction horizon as shown in Figure 6. As a result, three scenario tree of the outside temperature is generated as illustrated in Figure 7 and employed to solve the OCP for multistage MPC.

B. SIMULATION RESULT

This section presents the simulation results through figures comparing and explaining the performance of the four types of MPCs listed in Table 4.

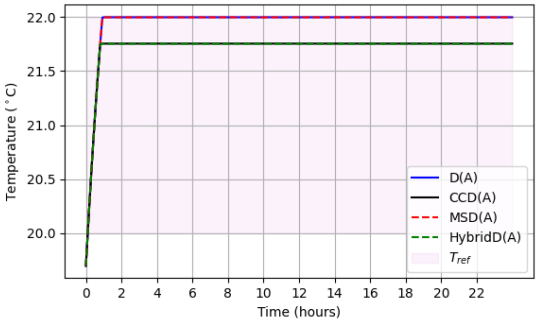

FIGURE 8. Temperature inside of the building (T_b) changes during the simulations of four types of MPCs: Deterministic MPC, Multistage MPC, Chance-constrained MPC, and Hybrid MPC with weight parameters as A in Table. 5, denoted as D(A), MS(A), CC(A), and Hybrid(A) respectively.

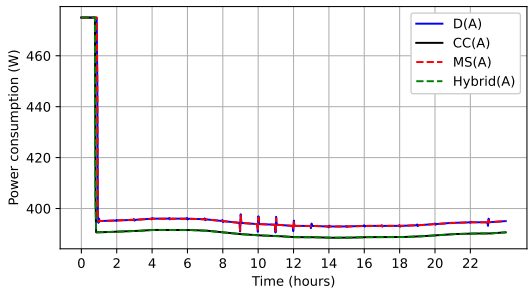

FIGURE 9. Electricity consumption by each type of MPC during the simulation period: Deterministic MPC, Multistage MPC, Chance-constrained MPC, and Hybrid MPC with weight parameters as A in Table. 5, denoted as D(A), MS(A), CC(A), and Hybrid(A) respectively.

Figure 8 and Figure 9 depict the change in the temperature inside the building T_b and the electricity consumption $\dot{Q}$ during the simulations of the Deterministic MPC, Multistage MPC, Chance-Constrained MPC, and Hybrid MPC with weight parameters set as A in Table 5, denoted as **D(A)**, **MS(A)**, **CC(A)**, and **Hybrid(A)**, respectively. Both figures show that all MPCs begin by actively heating the building from the initial temperature until it reaches a certain level. Accordingly, the electricity consumption is at its peak initially and then drops to a certain level to maintain the desired temperature inside the building. **D(A)** and **MS(A)** demonstrate similar performance. **CC(A)** and **Hybrid(A)** exhibit similar performance as well. However, due to the constrained back-off from model uncertainty, **CC(A)** and **Hybrid(A)** show more conservative performance than **D(A)** and **MS(A)**. Also, upon closer inspection in Figure 10, the

differences, between **D(A)** and **MS(A)** or between **CC(A)** and **Hybrid(A)**, become more apparent.

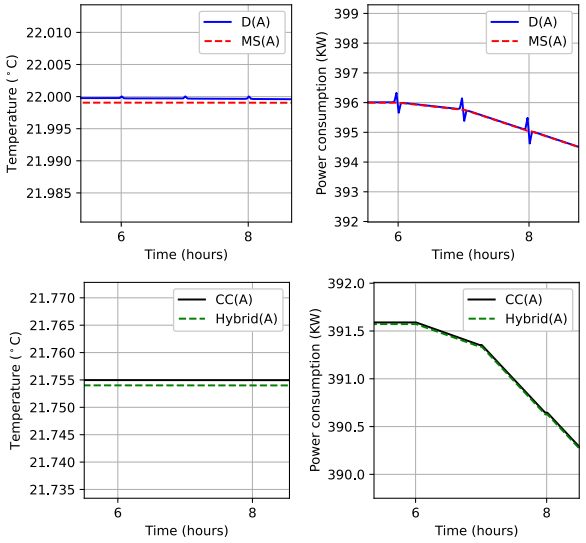

FIGURE 10. Detailed plots of the changes of the temperature inside of the building (T_b) and the electricity consumption in the building between 6 and 8 hours of simulations period: Deterministic MPC(D(A)), Multistage MPC(MS(A)), Chance-constrained MPC(CC(A)), and Hybrid MPC(Hybrid(A)) with weight parameters as A in Table. 5.

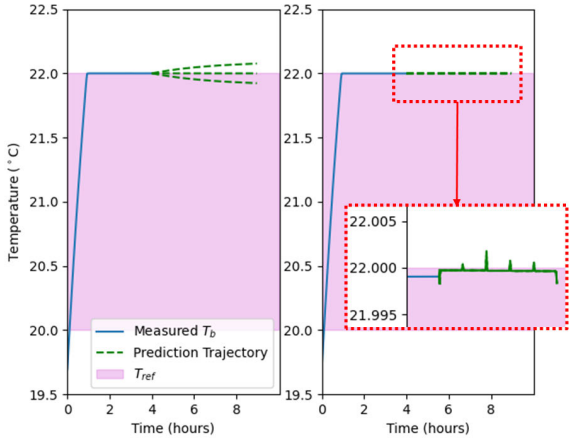

FIGURE 11. Prediction trajectories of T_b with the different realization of the weather forecast scenarios at 4 hours of the simulation period: (Left) Deterministic MPC, (Right) Multistage MPC with weight parameters as A in Table. 5.

Figure 10 provides detailed plots of the temperature changes and electricity consumption between 6 and 8 hours of the simulation period. The **MS(A)** shows a slightly more conservative performance compared to **D(A)**, as it considers the uncertainty of the outside temperature. Similarly, **Hybrid(A)** shows a more conservative performance compared to **CC(A)**. Figure 11 depicts the trajectories of the predicited temperature inside of the building based on three scenarios of the external temperature and control sequences from solving the OCPs during the middle of the simulation. The left plot in Figure 11 is simulated by **D(A)**. When the different scenario of the external temperature is realized, it shows the potential of the violation in the constraint. However, **MS(A)**, in the right plot, mitigate the violations. Upon closer inspection, it shows subtle violations, but it is a numerical error from solving the OCP iteratively. Figure 11 demonstrates the role of multistage MPC framework in both **MS(A)** and **Hybrid(A)** with the robustness of the satisfaction of the constraint against the influence of the uncertainty in the weather forecast information.

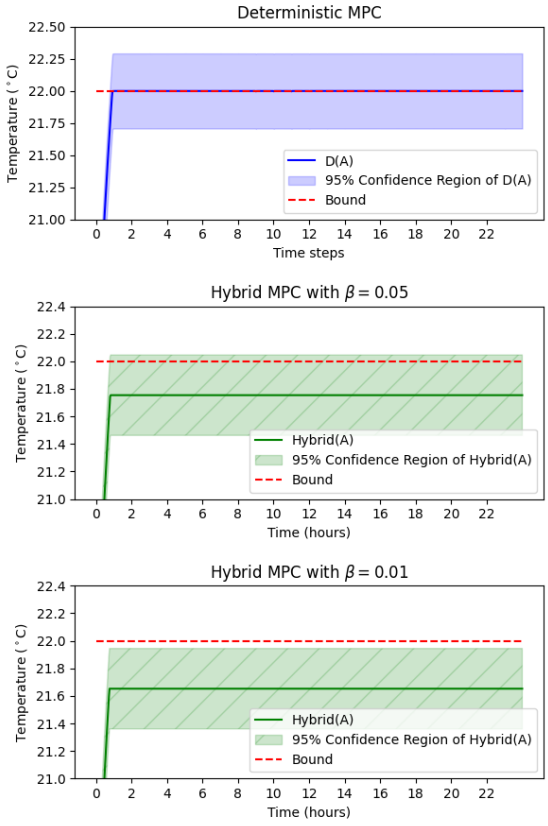

FIGURE 12. Comparison between the 95% confidence regions of Determisitic MPC(D), Hybrid MPC with $\beta = 0.05$, and Hybrid MPC with $\beta = 0.01$. The weight parameters of both MPCs are set as A in Table. 5.

Figure 12 presents a comparison of the 95% confidence regions of the model uncertainty between **D(A)** and **Hybrid(A)** with different values of β. In Figure 12, **D(A)** shows 50% of the 95% confidence region is out of the desired temperature bound. However, in Figure 12, bfHybrid(A) with $\beta = 0.05$ shows some robustness since the constraint is backed-off. When *beta* is set smaller as $\beta = 0.01$, the constraint is more backed off and it shows better robustness in the satisfaction of the constraint.

Table 6 reports the computational time required for solving the optimization problem on each MPC throughout simulations. The Deterministic MPC is the fastest, followed by the Chance-Constrained MPC, the Multistage MPC, and finally, the Hybrid MPC. However, all MPCs demonstrate similar computation times without significant differences in the matter of seconds.

TABLE 6. Computational time [s].

	Mean	Min	Max
Determinic MPC	0.2012	0.1650	0.3944
Multistage MPC	0.2376	0.2040	0.5910
Chance-constrained MPC	0.2185	0.1742	0.4410
Hybrid MPC	0.2637	0.2219	0.5940

By setting the weight parameters differently, the operation can be performed based on a preferred balance between setting the temperature at the set point and considering the electricity price. Figure 13 shows the simulations of the Hybrid MPC over a 5-day period with $\beta = 0.05$ and different sets of weight parameters (B, C, D, and E) from Table 5. As the weight parameter for temperature targeting (W_x) becomes relatively smaller compared to the electricity consumption weight (W_u), the temperature control becomes more influenced by the electricity price. For example, the Hybrid MPC with weight parameter set E (**Hybrid(E)**) displays an increase in temperature at around 40, 60, and 80 hours during the simulation period when the electricity price is relatively lower, as shown in Figure 5.

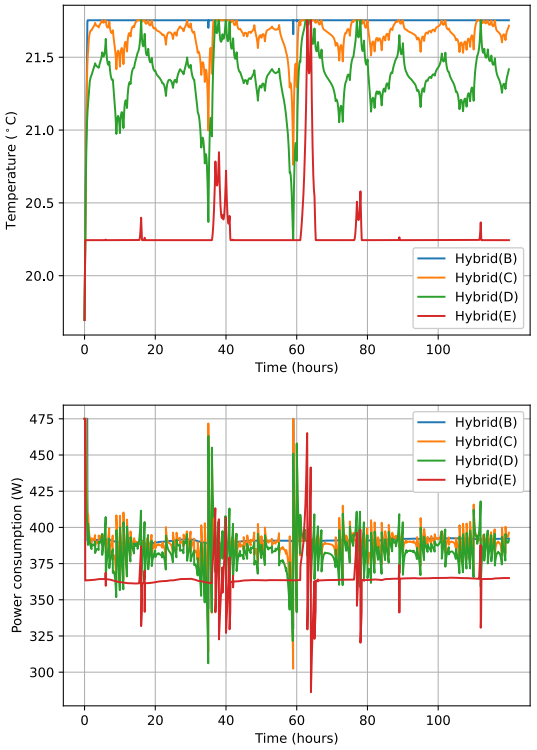

FIGURE 13. Simulations of the Hybrid MPC on the temperature inside of the building (T_b) with $\beta = 0.05$ and different sets of weight parameters: B, C, D, and E in Table.5.

Table.7 shows the total power consumptions and energy costs for the 5 days simulations on hybrid MPCs with different settings as shown in Figure 13. When the weight parameter W_u is relatively larger, less energy is used, and since the objective function (17) reflects the electricity price, it shows even less cost of the energy relatively compared to the reduction of the energy use.

TABLE 7. Power consumption and its cost throughout the 5 days simulations of Hybrid MPCs with different sets of weight parameters: B, C, D, and E in Table.5.

	Power consumption [Wh]	Cost [NOK]
Hybrid(B)	46976.42 (100%)	4.235 (100%)
Hybrid(C)	46777.44 (99.57%)	4.213 (99.46%)
Hybrid(D)	46120.70 (98.17%)	4.148 (97.93%)
Hybrid(E)	43744.33 (93.11%)	3.937 (92.94%)

VI. DISCUSSION

This paper implemented the simulation of various MPCs including the proposed hybrid MPC on a grey-box model of a building system for temperature control. Due to the mismatch between the model and the reality and the uncertainty in weather forecasts, it is not easy to keep the temperature inside the desired range. This may not be a significant concern in a small residential building over short periods, as human may not feel the difference of the temperature by 0.5°C. However, it may become more critical when considering long-term periods or different places such as large public buildings or important laboratories where constraint satisfaction is crucial. The hybrid MPC framework demonstrated a more conservative performance and exhibited higher robustness in satisfying the constraints by considering both uncertainties in the model and the weather forecast.

VII. CONCLUSION

In conclusion, the hybrid MPC, which is the combination of the multistage MPC and chance-constrained MPC frameworks, provides an effective robust approach for temperature control in buildings, particularly in scenarios where constraint satisfaction and robustness are of utmost importance. Further research can explore a method to improve the accuracy of the model by adaptive methods over the running time or additional variations of the hybrid framework and investigate its applicability in different building types and operational contexts.

REFERENCES

[1] IEA. *Buildings*. Paris, France. Accessed: Jun. 24, 2023. [Online]. Available: https://www.iea.org/reports/buildings
[2] T. Berthou, P. Stabat, R. Salvazet, and D. Marchio, "Development and validation of a gray box model to predict thermal behavior of occupied office buildings," *Energy Buildings*, vol. 74, pp. 91–100, May 2014, doi: 10.1016/j.enbuild.2014.01.038.
[3] M. Morari and J. H. Lee, "Model predictive control: Past, present and future," *Comput. Chem. Eng.*, vol. 23, pp. 667–682, Jan. 1999, doi: 10.1016/S0098-1354(98)00301-9.
[4] D. Q. Mayne, J. B. Rawlings, C. V. Rao, and P. O. M. Scokaert, "Constrained model predictive control: Stability and optimality," *Automatica*, vol. 36, no. 6, pp. 789–814, 2000, doi: 10.1016/S0005-1098(99)00214-9.
[5] C. A. Thilker, H. G. Bergsteinsson, P. Bacher, H. Madsen, D. Calì, and R. G. Junker, "Non-linear model predictive control for smart heating of buildings," in *Proc. E3S Web Conf.*, vol. 246, 2021, p. 9005.
[6] C. A. Thilker, H. Madsen, and J. B. Jørgensen, "Advanced forecasting and disturbance modelling for model predictive control of smart energy systems," *Appl. Energy*, vol. 292, Jun. 2021, Art. no. 116889, doi: 10.1016/j.apenergy.2021.116889.

[7] F. Oldewurtel, A. Parisio, C. N. Jones, D. Gyalistras, M. Gwerder, V. Stauch, B. Lehmann, and M. Morari, "Use of model predictive control and weather forecasts for energy efficient building climate control," *Energy Buildings*, vol. 45, pp. 15–27, Feb. 2012, doi: 10.1016/j.enbuild.2011.09.022.

[8] T. Hilliard, L. Swan, and Z. Qin, "Experimental implementation of whole building MPC with zone based thermal comfort adjustments," *Building Environ.*, vol. 125, pp. 326–338, Nov. 2017, doi: 10.1016/j.buildenv.2017.09.003.

[9] S. Prívara, J. Cigler, Z. Váňa, F. Oldewurtel, C. Sagerschnig, and E. Žáčeková, "Building modeling as a crucial part for building predictive control," *Energy Buildings*, vol. 56, pp. 8–22, Jan. 2013, doi: 10.1016/j.enbuild.2012.10.024.

[10] D. W. U. Perera, C. F. Pfeiffer, and N.-O. Skeie, "Modelling the heat dynamics of a residential building unit: Application to Norwegian buildings," *Model., Identificat. Control, Norwegian Res. Bull.*, vol. 35, no. 1, pp. 43–57, 2014, doi: 10.4173/mic.2014.1.4.

[11] L. Ljung, "Prediction error estimation methods," *Circuits, Syst., Signal Process.*, vol. 21, no. 1, pp. 11–21, Jan. 2002, doi: 10.1007/BF01211648.

[12] M. J. Jiménez, H. Madsen, and K. K. Andersen, "Identification of the main thermal characteristics of building components using MATLAB," *Building Environ.*, vol. 43, no. 2, pp. 170–180, Feb. 2008, doi: 10.1016/j.buildenv.2006.10.030.

[13] K. H. Esbensen, D. Guyot, F. Westad, and L. P. Houmller, *Multivariate Data Analysis: In Practice: An Introduction to Multivariate Data Analysis and Experimental Design*, 5th ed. Oslo, Norway: CAMO, 2010, ch. 6, sec. 9, pp. 137–147.

[14] D. W. U. Perera, M. Halstensen, and N.-O. Skeie, "Prediction of space heating energy consumption in cabins based on multivariate regression modelling," *Int. J. Model. Optim.*, vol. 5, no. 6, pp. 385–392, 2015, doi: 10.7763/IJMO.2015.V5.493.

[15] S. F. Fux, A. Ashouri, M. J. Benz, and L. Guzzella, "EKF based self-adaptive thermal model for a passive house," *Energy Buildings*, vol. 68, pp. 811–817, Jan. 2014, doi: 10.1016/j.enbuild.2012.06.016.

[16] A. Afram and F. Janabi-Sharifi, "Gray-box modeling and validation of residential HVAC system for control system design," *Appl. Energy*, vol. 137, pp. 134–150, Jan. 2015, doi: 10.1016/j.apenergy.2014.10.026.

[17] G. Reynders, J. Diriken, and D. Saelens, "Quality of grey-box models and identified parameters as function of the accuracy of input and observation signals," *Energy Buildings*, vol. 82, pp. 263–274, Oct. 2014, doi: 10.1016/j.enbuild.2014.07.025.

[18] N. R. Kristensen, H. Madsen, and S. B. Jørgensen, "Parameter estimation in stochastic grey-box models," *Automatica*, vol. 40, no. 2, pp. 225–237, Feb. 2004, doi: 10.1016/j.automatica.2003.10.001.

[19] *Thermal Network Modelling Handbook*, NASA, Washington, DC, USA, 1972, ch. 2, pp. 3–68.

[20] M. J. Jiménez, H. Madsen, J. J. Bloem, and B. Dammann, "Estimation of non-linear continuous time models for the heat exchange dynamics of building integrated photovoltaic modules," *Energy Buildings*, vol. 40, no. 2, pp. 157–167, Jan. 2008, doi: 10.1016/j.enbuild.2007.02.026.

[21] O. M. Brastein, A. Ghaderi, C. F. Pfeiffer, and N.-O. Skeie, "Analysing uncertainty in parameter estimation and prediction for grey-box building thermal behaviour models," *Energy Buildings*, vol. 224, Oct. 2020, Art. no. 110236, doi: 10.1016/j.enbuild.2020.110236.

[22] O. M. Brastein, D. W. U. Perera, C. Pfeifer, and N.-O. Skeie, "Parameter estimation for grey-box models of building thermal behaviour," *Energy Buildings*, vol. 169, pp. 58–68, Jun. 2018, doi: 10.1016/j.enbuild.2018.03.057.

[23] A. Mesbah, "Stochastic model predictive control: An overview and perspectives for future research," *IEEE Control Syst. Mag.*, vol. 36, no. 6, pp. 30–44, Dec. 2016, doi: 10.1109/MCS.2016.2602087.

[24] Y. Ma, S. Vichik, and F. Borrelli, "Fast stochastic MPC with optimal risk allocation applied to building control systems," in *Proc. IEEE 51st IEEE Conf. Decis. Control (CDC)*, Maui, HI, USA, Dec. 2012, pp. 7559–7564, doi: 10.1109/CDC.2012.6426251.

[25] M. Cannon, B. Kouvaritakis, and X. Wu, "Probabilistic constrained MPC for multiplicative and additive stochastic uncertainty," *IEEE Trans. Autom. Control*, vol. 54, no. 7, pp. 1626–1632, Jul. 2009, doi: 10.1109/TAC.2009.2017970.

[26] P. Li, M. Wendt, and G. Wozny, "Robust model predictive control under chance constraints," *Comput. Chem. Eng.*, vol. 24, no. 2, pp. 829–834, 2000, doi: 10.1016/S0098-1354(00)00398-7.

[27] I. Jurado, P. Millán, D. Quevedo, and F. R. Rubio, "Stochastic MPC with applications to process control," *Int. J. Control*, vol. 88, pp. 792–800, Apr. 2015, doi: 10.1080/00207179.2014.975845.

[28] L. Blackmore, M. Ono, and B. C. Williams, "Chance-constrained optimal path planning with obstacles," *IEEE Trans. Robot.*, vol. 27, no. 6, pp. 1080–1094, Dec. 2011, doi: 10.1109/TRO.2011.2161160.

[29] A. Gray, Y. Gao, T. Lin, J. K. Hedrick, and F. Borrelli, "Stochastic predictive control for semi-autonomous vehicles with an uncertain driver model," in *Proc. 16th Int. IEEE Conf. Intell. Transp. Syst. (ITSC)*, Hague, The Netherlands, Oct. 2013, pp. 2329–2334, doi: 10.1109/ITSC.2013.6728575.

[30] M. Maiworm, T. Bäthge, and R. Findeisen, "Scenario-based model predictive control: Recursive feasibility and stability," *IFAC-PapersOnLine*, vol. 48, no. 8, pp. 50–56, 2015, doi: 10.1016/j.ifacol.2015.08.156.

[31] C. Jeong, B. Furenes, and R. Sharma, "Multistage model predictive control with simplified scenario ensembles for robust control of hydropower station," *Model., Identificat. Control, Norwegian Res. Bull.*, vol. 44, no. 2, pp. 43–54, 2023, doi: 10.4173/mic.2023.2.1.

[32] P. O. M. Scokaert and D. Q. Mayne, "Min-max feedback model predictive control for constrained linear systems," *IEEE Trans. Autom. Control*, vol. 43, no. 8, pp. 1136–1142, Aug. 1998, doi: 10.1109/9.704989.

[33] S. Lucia, T. Finkler, and S. Engell, "Multi-stage nonlinear model predictive control applied to a semi-batch polymerization reactor under uncertainty," *J. Process Control*, vol. 23, no. 9, pp. 1306–1319, Oct. 2013, doi: 10.1016/j.jprocont.2013.08.008.

[34] E. Klintberg, J. Dahl, J. Fredriksson, and S. Gros, "An improved dual Newton strategy for scenario-tree MPC," in *Proc. IEEE 55th Conf. Decis. Control (CDC)*, Las Vegas, NV, USA, Dec. 2016, pp. 3675–3681, doi: 10.1109/CDC.2016.7798822.

[35] A. T. Schwarm and M. Nikolaou, "Chance-constrained model predictive control," *AIChE J.*, vol. 45, no. 8, pp. 1743–1752, Aug. 1999, doi: 10.1002/aic.690450811.

[36] T. A. N. Heirung, J. A. Paulson, J. O'Leary, and A. Mesbah, "Stochastic model predictive control—How does it work?" *Comput. Chem. Eng.*, vol. 114, pp. 158–170, Jun. 2018, doi: 10.1016/j.compchemeng.2017.10.026.

[37] M. J. D. Powell, "A direct search optimization method that models the objective and constraint functions by linear interpolation," in *Advances in Optimization and Numerical Analysis*, vol. 275, 1994, pp. 51–67, doi: 10.1007/978-94-015-8330-5_4.

[38] P. Bacher and H. Madsen, "Identifying suitable models for the heat dynamics of buildings," *Energy Buildings*, vol. 43, no. 7, pp. 1511–1522, Jul. 2011, doi: 10.1016/j.enbuild.2011.02.005.

[39] A. Simpkins, "System identification: Theory for the user, 2nd edition (Ljung, L.; 1999) [on the shelf]," *IEEE Robot. Autom. Mag.*, vol. 19, no. 2, pp. 95–96, Jun. 2012, doi: 10.1109/MRA.2012.2192817.

[40] D. Perera and N.-O. Skeie, "Estimation of the heating time of small-scale buildings using dynamic models," *Buildings*, vol. 6, no. 1, p. 10, Mar. 2016, doi: 10.3390/buildings6010010.

[41] J. A. E. Andersson, J. Gillis, G. Horn, J. B. Rawlings, and M. Diehl, "CasADi: A software framework for nonlinear optimization and optimal control," *Math. Program. Comput.*, vol. 11, no. 1, pp. 1–36, Mar. 2019, doi: 10.1007/s12532-018-0139-4.

CHANGHUN JEONG received the B.S. degree in chemical engineering from the University of Ulsan, South Korea, in 2016, and the M.S. degree in chemical engineering from the Norwegian University of Science and Technology, Norway, in 2020. He is currently pursuing the Ph.D. degree with the University of South-Eastern Norway. His research interests include the applications of the model predictive control on hydropower systems and HVAC systems under the presence of uncertainties.

OLE MAGNUS BRASTEIN received the M.Sc. degree in systems and control engineering and the Ph.D. degree in parameter estimation and machine learning from the University of South-Eastern Norway, in 2016 and 2020, respectively. Industrial research and development background, since 2004, in a wide range of projects, from hardware/instrumentation, to software engineering, and embedded systems. His research interests include software design and development, machine learning, artificial intelligence, estimation algorithms, and creative research and development process.

NILS-OLAV SKEIE received the M.Sc. degree in computer architecture, computer network, and instrumentation and the Ph.D. degree in soft sensors for level estimation from the Norwegian University of Science and Technology, in 1985 and 2008, respectively. With abundant industrial experience, he has been a Professor, since 2006, with the University of South-Eastern Norway (Previously, Telemark University College). His research interests include machine learning, data-driven models, soft sensors, empirical models, digitalization, software engineering, smart buildings, building energy management systems (BEMS), building automation systems (BAS), welfare technology, systems design, level measurement systems, instrumentation technologies, measurement systems (DAQ), process control systems (SCADA/IT/OT), industry 4.0, and smart production.

ROSHAN SHARMA received the Ph.D. degree in process, energy, and automation from the Telemark University College, in 2014. He is currently an Associate Professor with the University of South-Eastern Norway, Norway. He has been a researcher within the energy-related industries, since 2011. His research interests include model-based advanced control, process optimization, and state and parameter estimation.